1521-0111/96/2/148–157$35.00
MOLECULAR PHARMACOLOGY

https://doi.org/10.1124/mol.119.116640
Mol Pharmacol 96:148–157, August 2019

The L46P Mutant Confers a Novel Allosteric Mechanism of Resistance Toward the Influenza A Virus M2 S31N Proton Channel Blockers

Rami Musharrafieh, Panagiotis I. Lagarias, Chunlong Ma, Gene S. Tan, Antonios Kolocouris, and Jun Wang

Department of Pharmacology and Toxicology, College of Pharmacy (R.M., C.M., J.W.) and Department of Chemistry and Biochemistry (R.M.), University of Arizona, Tucson, Arizona; Department of Pharmaceutical Chemistry, Faculty of Pharmacy, National and Kapodistrian University of Athens, Panepistimiopolis-Zografou, Greece (P.I.L., A.K.); J. Craig Venter Institute, La Jolla, California (G.S.T.); and Department of Medicine, University of California, San Diego, La Jolla, California (G.S.T.)

Received March 11, 2019; accepted May 30, 2019

ABSTRACT

The Food and Drug Administration–approved influenza A antiviral amantadine inhibits the wild-type (WT) AM2 channel but not the S31N mutant predominantly found in circulating strains. In this study, serial viral passages were applied to select resistance against a newly developed isoxazole-conjugated adamantane inhibitor that targets the AM2 S31N channel. This led to the identification of the novel drug-resistant mutation L46P located outside the drug-binding site, which suggests an allosteric resistance mechanism. Intriguingly, when the L46P mutant was introduced to AM2 WT, the channel remained sensitive toward amantadine inhibition. To elucidate the molecular mechanism, molecular dynamics simulations and binding free energy molecular mechanics–generalized born surface area (MM-GBSA) calculations were performed on WT and mutant channels. It was found that the L46P mutation caused a conformational change in the N terminus of transmembrane residues 22–31 that ultimately broadened the drug-binding site of AM2 S31N inhibitor **4**, which spans residues 26–34, but not of AM2 WT inhibitor amantadine, which spans residues 31–34. The MM-GBSA calculations showed stronger binding stability for **4** in complex with AM2 S31N compared with **4** in complex with AM2 S31N/L46P, and equal binding free energies of amantadine in complex with AM2 WT and AM2 L46P. Overall, these results demonstrate a unique allosteric resistance mechanism toward AM2 S31N channel blockers, and the L46P mutant represents the first experimentally confirmed drug-resistant AM2 mutant that is located outside of the pore where drug binds.

SIGNIFICANCE STATEMENT

AM2 S31N is a high-profile antiviral drug target, as more than 95% of currently circulating influenza A viruses carry this mutation. Understanding the mechanism of drug resistance is critical in designing the next generation of AM2 S31N channel blockers. Using a previously developed AM2 S31N channel blocker as a chemical probe, this study was the first to identify a novel resistant mutant, L46P. The L46P mutant is located outside of the drug-binding site. Molecular dynamics simulations showed that L46P causes a dilation of drug-binding site between residues 22 and 31, which affects the binding of AM2 S31N channel blockers, but not the AM2 WT inhibitor amantadine.

Introduction

AM2 is a proton-selective ion channel essential for the replication of influenza A viruses (Pinto et al., 1992; Takeda et al., 2002; Wang et al., 2015). The AM2 channel is a homotetrameric transmembrane protein with 97 residues per monomer. The N-terminal domain (residues 1–23) is largely unstructured with polar residues that help increase the hydration of the pore to facilitate proton conductance (Kwon and Hong, 2016; Ma and Wang, 2018) and for incorporation into virions (Park et al., 1998). The transmembrane (TM) domain (residues 24–43) is required for the formation of a left-handed 4-helix bundle (Cady and Hong, 2008; Stouffer et al., 2008) and for both proton conductance and selectivity (Balannik et al., 2010) as well as drug binding (Ma et al., 2009). In the TM domain, a conserved H37XXXW41 motif forms the selectivity filter and accounts for proton gating. Four histidine side chain imidazole groups at residue 37 face towards the pore region of the channel and are protonated sequentially, resulting in pH activation and proton selectivity (Acharya et al., 2010; Hu et al., 2010). Tryptophan

This research was supported by the National Institutes of Health (NIH) [Grants AI119187 and AI144887 to J.W.]. We thank Chiesi Hellas, which supported this research (Special Account for Research Grants [SARG] No. 10354), and the State Scholarships Foundation (IKY) for providing a Ph.D. fellowship to P.I.L. (MIS 5000432, NSRF 2014–2020). This project was partly funded with federal funds from the NIH National Institute of Allergy and Infectious Diseases, Department of Health and Human Services [Award Number U19AI110819].
https://doi.org/10.1124/mol.119.116640.

ABBREVIATIONS: MD, molecular dynamics; MDCK, Madin-Darby canine kidney; MDCK-ST6Gal I, MDCK cells overexpressing ST6Gal I; MM-GBSA, molecular mechanics–generalized born surface area; NPT, XXX; P0, passage 0; P4, passage 04; P5, passage 05; PCR, polymerase chain reaction; PDB, Protein Data Bank; POPC, 1-palmitoyl-2-oleoyl-glycero-3-phosphocholine; TEVC, two-electrode voltage clamp; TM, transmembrane; WT, wild-type.

41 acts as a gate to help drive unidirectional conductance from the N terminus to the C terminus (Tang et al., 2002; Ma et al., 2013). The remaining residues 44–97 contain a cytoplasmic amphiphilic helix (44–60) that is responsible for virus budding and scission (Chen et al., 2008; Rossman et al., 2010; Schmidt et al., 2013) and a C-terminal tail (61–97) that binds to the viral matrix protein M1 (McCown and Pekosz, 2006).

Amantadine inhibits influenza A virus replication by blocking the AM2 wild-type (WT) channel. The drug-binding site was determined to be the pore region between residues 27 and 34 (Cady et al., 2010; Thomaston et al., 2018). This pore-blocking model placed the adamantane (**1**) cage near serine 31 with the polar ammonium group facing the histidine 37 tetrad (Fig. 2A). Clinical use of amantadine was phased out due to prevailing drug resistance among circulating viruses. Therefore, it is equally important to study the mechanisms of resistance as the mechanisms of action. The standard method of elucidating drug resistance in the laboratory is to generate escape variants by passaging the virus with increasing antiviral selection pressure. For AM2 WT, mutations L26F, V27A, A30T, S31N, and G34E have emerged as a result of amantadine selection (Wang et al., 2015; Wang, 2016). Of note, all of these mutations were located in the AM2 pore region at the amantadine drug-binding area.

Several isoxazole-conjugated amantadine analogs (**2–6**) have been developed to inhibit the AM2 S31N mutant channel in electrophysiological and in vitro antiviral assays (Wang et al., 2013b, 2018; Li et al., 2017). The drug-binding site and mechanism of action of 19 S31N inhibitors were determined by both solution and solid-state NMR (Fig. 2B) (Wang et al., 2013b; Wu et al., 2014). Interestingly, AM2 S31N inhibitors bind to the AM2 S31N channel with a flipped orientation compared with amantadine in the AM2 WT channel: the hydrophobic adamantane cage is located at the hydrophobic pocket created by G34, and the isoxazole interacts with residues V26 and N31 through side chain hydrophobic interactions and backbone hydrogen bonding, respectively.

The emergence of drug resistance was previously profiled for several potent AM2 S31N inhibitors (Ma et al., 2016; Musharrafieh et al., 2018). The mutations identified were single-mutant AM2 S31N/L26I, AM2 S31N/V27I, or the double-mutant AM2 S31N/L26I/A30T. Molecular modeling showed that the V27I and A30T mutants prevent drug binding directly through pore constriction or changes in the polarity of the channel. Residue 26 is located at the helical interface, and the L26I mutation was postulated to change the local structure of the channel, leading to drug resistance.

Compound **4** was recently developed with optimized in vitro pharmacokinetic properties based on structure-property relationship studies (Wang et al., 2018). To advance this lead compound further, it is critical to understand its mechanism of resistance. As such, in the present work, serial viral passage experiments were performed with compound **4** using the 2009 H1N1 pandemic influenza A virus, A/California/07/2009. The unusual mutant L46P was identified and led to resistance to **4**. Electrophysiological experiments showed that the AM2 S31N/L46P channel is not blocked by compound **4** nor previously developed AM2 S31N inhibitors (**2**, **3**, **5**, and **6**) but remained functional as a proton-selective channel. The resistance mechanism of AM2 S31N/L46P against compound **4** as well as the effect of AM2 L46P on amantadine inhibition was further investigated using molecular dynamics (MD) simulations and molecular mechanics–generalized born surface area (MM-GBSA) calculations.

Materials and Methods

Cell Lines and Viruses. Madin-Darby canine kidney (MDCK) cells were maintained at 37°C in a 5% CO_2 atmosphere using standard cell culture procedures. MDCK cells overexpressing ST6Gal I (MDCK-ST6Gal I) were cultured in the presence of 7.5 μg/ml puromycin. Influenza A virus strain A/California/07/2009 (H1N1) was amplified in MDCK-ST6Gal I and stored at −80°C with 0.5% bovine serum albumin prior to use.

Antiviral Assays. Antiviral experiments were performed using the plaque-reduction assay as previously described (Ma et al., 2016; Musharrafieh et al., 2018). In brief, a confluent monolayer of MDCK-ST6Gal I was infected with ~100 plaque-forming unit of H1N1 diluted in Dulbecco's modified Eagle's medium with 0.5% bovine serum albumin. Infection was synchronized at 4°C for around 1 hour, then transferred to a 37°C incubator for 1 hour. Infectious medium was subsequently removed, and cells were washed with PBS. Cells were overlaid with Dulbecco's modified Eagle's medium, N-acetyl trypsin (2.0 μg/ml), and 1.2% avicel microcrystalline cellulose and incubated until plaque formation became visible after crystal violet staining (around 2 days after infection). The half-maximal effective concentration (EC_{50}) values were calculated by determining the total plaque area in each well using ImageJ software (National Institutes of Health). Serial passage experiments were performed using a viral titer of 0.001 multiplicity of infection as previously described (Musharrafieh et al., 2018).

M2 Sequencing. The M2 gene from each passage was sequenced by first extracting the viral RNA using a QIAamp viral RNA Mini Kit (Qiagen, Hilden, Germany). The purified viral RNA was reverse transcribed, and a polymerase chain reaction (PCR) using M-specific primers (5′-TAGATATTAAAGATGAGTCTTC-3′ and 5′-CTCTAGCTCTATGTTGACAAAATGACC-3′) was used to amplify the gene segment. The PCR product was run on a 1% agarose gel, extracted, and purified using a Wizard SV Gel and PCR Clean-up System (Promega, Madison, WI). M2 was sent to Eton Bioscience, Inc. for sequencing. Whole-genome sequencing of passaged viruses was performed by the J. Craig Venter Institute (La Jolla, CA). In brief, a one-step multisegment reverse-transcription and PCR amplification approach using virus-specific primers was used to generate amplicons (PMID: 19605485). Libraries were generated using sequence-independent single-primer amplification (PMID: 18179705) (with each sample double-barcoded) and sequenced on an Illumina MiSeq instrument (2 × 300 bp).

Electrophysiological Two-Electrode Voltage Clamp Assay. Female *Xenopus laevis* frogs were purchased from Nasco (Fort Atkinson, WI). Oocyte harvesting was performed according to protocol approved by the University of Arizona IACUC. Electrophysiological measurements were performed using the AM2 gene out of the A/California/07/2009 as previously described (Balannik et al., 2010; Musharrafieh et al., 2018). In brief, mRNA coding A/California/07/2009 AM2 and its variants were synthesized via an mMessage and mMachine T7 kit (Invitrogen) according to manufacturer protocol. Ten to 50 ng of mRNA was injected into each oocyte. Twenty-four to 72 hours after mRNA injection, electrophysiological two-electrode voltage clamp (TEVC) recordings were performed. Oocytes were constantly held at −20 mV, and current was recorded at various testing conditions. The detailed EC_{50} measurement was described by Jing et al. (2008). At least eight concentrations covering the EC_{50} value of each compound were applied in the TEVC recording. At least three oocytes were recorded at each concentration. The percentage of remaining channel current after application of compounds was plotted against the compound concentration with dose-response function in GraphPad Prism 5.0.

The AM2 channel–specific conductance was measured as described by Musharrafieh et al. (2018). In brief, the membrane currents of

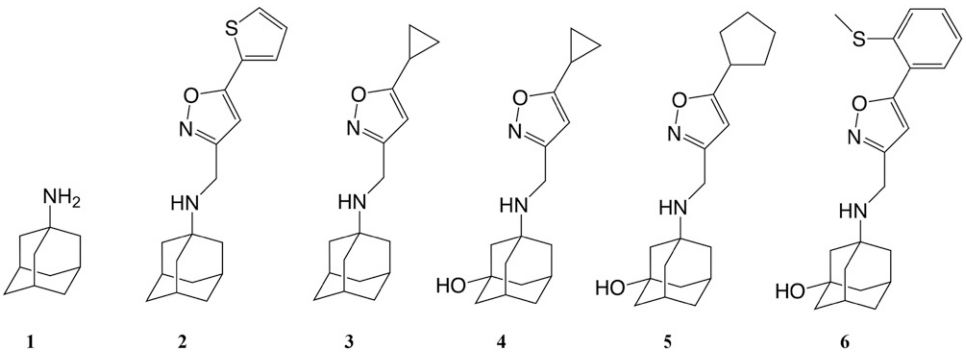

Fig. 1. AM2 WT inhibitor amantadine (**1**) and the AM2 S31N inhibitors 2–6.

individual oocytes expressing A/California/07/2009 AM2 or its mutants were first recorded with TEVC electrophysiology technique. Eight to 10 oocytes expressing AM2 or L46P mutant recorded with different currents were saved and fixed with 2% paraformaldehyde for 30 minutes. Fixed whole oocytes were immunostained with primary 14C2 (anti-AM2; gift from Dr. Robert A. Lamb, Northwestern University, Evanston, IL) monoclonal antibody and secondary Alexa Fluor 546–labeled goat anti-mouse IgG (Molecular Probes, Inc., Medford, OR). A ZOE fluorescent Cell Imager (Bio-Rad) was used to acquire fluorescence images, and about one-half of the surface of each oocyte was imaged. Photoshop was used to quantify the fluorescence intensity by measuring the gray-scale value. As a control for the autofluorescence signal from the yolk, uninjected oocytes were measured. The relative specific activity of AM2 was obtained by taking the slope of the linear regression curve generated from plotting the whole-cell current against the AM2 expression level (detected by immunofluorescence) for each oocyte.

The L46P mutation was introduced using site-directed mutagenesis (QuikChange Site-Directed Mutagenesis Kit; Agilent, Santa Clara, CA).

Protein Preparation: Docking Calculations. The structure of (**4**) was built with a Schrödinger 2017-1 platform (Schrödinger Release 2018-1: Maestro; Schrödinger, LLC, New York, NY) and minimized by the conjugate gradient method using the MMFF94 force field (Halgren, 1996) and a distance-dependent dielectric constant of 4.0 until a convergence threshold of 0.0001 kJ mol^{-1} $Å^{-1}$ was reached. The Protein Data Bank (PDB) ID 2L0J was used for AM2 WT (22–62) *apo* protein. N and C termini of the AM2 WT (22–62) model systems were capped by acetyl and methylamino groups. After applying the protein preparation module of Maestro [Schrödinger Release 2017-1: Maestro (Schrödinger) and Maestro, version 8.5 (Schrodinger, Inc., New York, NY)], all hydrogens of the protein complex were minimized with the AMBER* force field by means of Maestro/Macromodel 9.6 using a distance-dependent dielectric constant of 4.0. The molecular mechanics minimizations were performed with a conjugate gradient method and a threshold value of 0.0001 kJ $Å^{-1}$ mol^{-1} as the convergence criterion. AM2 S31N (22–62) protein was obtained by manual mutation of S31 to N31. MD simulations of AM2 S31N (22–62) in hydrated 1-palmitoyl-2-oleoyl-glycero-3-phosphocholine (POPC) for 1 μs produced a well equilibrated *apo* protein AM2 S31N structure. The simulated AM2 S31N (22–62) *apo* protein was superimposed with AM2 S31N (19–49) in complex with compound **2** (M2WJ332) (PDB: 2LY0) (Wang et al., 2013b), which after deletion of AM2 S31N (19–49) resulted in a complex of AM2 S31N (22–62) with **2**. The structures of the protein AM2 S31N (22–62) and ligand **2** were saved separately and were used for the subsequent docking calculations of ligand **4** to AM2 S31N (22–62) with GOLD 5.2 (The Cambridge Crystallographic Data Centre) (Jones et al., 1997), using the GoldScore scoring function (Verdonk et al., 2005). The region of interest used by GOLD was defined to contain the atoms that were within ~15 Å of the compound **1** binding site in the structure. For all of the parameters of GOLD 5.2, default values were used, apart from the "allow early termination" that was skipped. Ligand **4** was submitted to 30 genetic algorithm runs. Ten docking poses were produced which were visually inspected using the University of California, San Francisco Chimera package (Pettersen et al., 2004). The docking pose with the best GoldScore score was used for the subsequent MD simulations. L46P was manually applied in the simulated AM2 S31N (22–62) to produce AM2 S31N/L46P *apo* protein. MD simulations of AM2 S31N/L46P in hydrated POPC for 1 μs produced a well equilibrated *apo* protein AM2 S31N/L46P structure; its complex with **4** was produced after docking **4** to AM2 S31N/L46P as described earlier. AM2 WT (22–62) was superimposed with AM2 WT (22–46)–**1** complex (PDB: 2KQT), which after deletion of AM2 WT (22–46) afforded the complex of AM2 WT (22–62) with compound **1**. The L46P mutation resulted in the AM2 L46P–**1** complex.

MD Simulations. The proteins AM2 S31N and AM2 S31N/L46P and the complexes AM2 S31N–**4**, AM2 S31N/L46P–**4**, and AM2 L46P–**1** were embedded in a hydrated POPC bilayer extending 10 × 10 × 20 $Å^3$ in the XYZ directions from the channel. For the membrane insertion and neutralization, the System Builder module of Desmond was used [Schrödinger Release 2018-1: Maestro (Schrödinger) and Desmond Molecular Dynamics System, version 3.0 (D.E. Shaw Research, New York, NY)]. Periodic boundary conditions were applied in 75 × 75 × 95 $Å^3$, including 107 POPC lipids. A 20-Å area above and below the protein included 9636 waters. The total number of atoms, including the protein inside the hydrated bilayer, was ~47,000. The

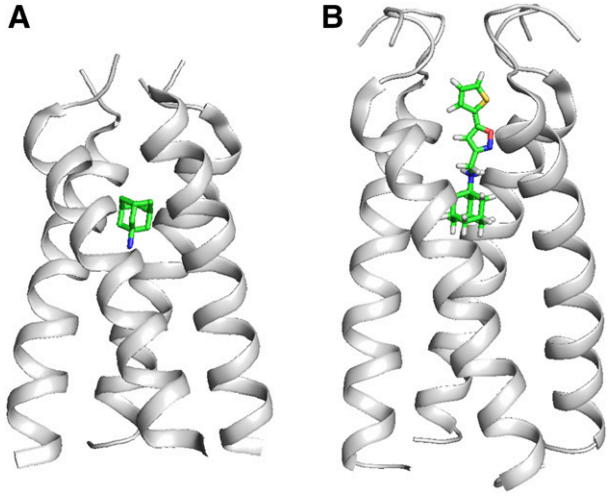

Fig. 2. AM2 inhibitors are a class of influenza antivirals that bind to the pore of the channel. (A) Influenza AM2 WT [Protein Data Bank (PDB): 6BKK] structure bound with amantadine (**1**) with the amino group oriented toward the C terminus. (B) Influenza AM2 S31N structure (PDB: 2LY0) in complex with compound (**2**) with the conjugated isoxazole group positioned at the N terminus.

systems were neutralized by adding Na^+ ions. A 0.15 M NaCl solution was added. Ligands **1** and **4** were positively charged (+1) using the Schrödinger 2017-1 Maestro platform. The H37 residues of the AM2 TM were protonated at Nε2 because this form was found to be the most populated, and four uncharged H37 residues were applied (Hu et al., 2010; Sharma et al., 2010). TIP3P (Jorgensen et al., 1983) was applied as the water model, and the Schrödinger's viparr utility was used to assign CHARMM36 parameters in protein, lipids, and ions (Best et al., 2012).

All simulations were run with the Desmond MD algorithm (Bowers et al., 2006), as implemented by Schrödinger [Schrödinger Release 2017-1: Desmond Molecular Dynamics System (D. E. Shaw Research, New York, NY) and Maestro-Desmond Interoperability Tools (Schrödinger)]. Particle mesh Ewald (PME) was used to calculate long-range electrostatic interactions (Darden et al., 1993; Essmann et al., 1995) with a grid spacing of 0.8 Å. The Shake method was used to keep all bonds with hydrogen rigid, at ideal lengths and angles (Ryckaert et al., 1977). Van der Waals and short-range electrostatic interactions were smoothly truncated at 9.0 Å. The Nosé-Hoover thermostat was used, and the Martyna-Tobias-Klein method (Martyna et al., 1994) was used for pressure control. The equations of motion were integrated using the multistep reversible reference system propagator algorithm integrator (Humphreys et al., 1994) with an inner time step of 2.0 femtoseconds for bonded interactions and nonbonded interactions within the cutoff. An outer time step of 6.0 femtoseconds was used for nonbonded interactions beyond the cutoff. Periodic boundary conditions were applied. For all MD simulations, the same relaxation protocol was used. In short, two rounds of steepest descent minimization were performed, one with a maximum of 2000 steps and a harmonic restraint of 50 kcal mol^{-1} $Å^{-2}$ on all heavy solute atoms and a second with 10,000 steps without restraints. Next, a series of MD simulations was performed. The first simulation was performed for 200 ps starting at 10 K with gradual heating until 310 K in the NVT ensemble with the solute heavy atoms restrained with a force constant of 50 kcal mol^{-1} $Å^{-2}$. A temperature of 308 K was used in our MD simulations to ensure that the membrane state was above the melting temperature state of POPC lipids (Koynova and Caffrey, 1998). The heating was followed by equilibration runs. One for 1000-ps simulation in the NPT ensemble with the solute heavy atoms restrained with a force constant of 10 kcal mol^{-1} $Å^{-2}$ to equilibrate solvent and lipids. Next, a 10-ns NPT ensemble simulation with 10 kcal mol^{-1} $Å^{-2}$ on solute atoms was run. Two NPT MD simulations, 1000 ps each, followed. In the first, harmonic constraints were gradually decreased from 10.0 to 2.0 kcal mol^{-1} $Å^{-2}$ on solute heavy atoms while retaining 2.0 kcal mol^{-1} $Å^{-2}$ constraints on all other solute atoms. Next, all harmonic constraints were removed except a 2.0-kcal mol^{-1} $Å^{-2}$ set on protein C_α atoms. This equilibration protocol was followed by an NPT simulation without restraints for 1 μs for the *apo* proteins and 100 ns for the complexes. The replicas of the system were saved every 10 ps. Within this simulation time, the total energy and root-mean-square-deviation of the protein backbone C_α atoms (Lyman and Zuckerman, 2006) reached a plateau, and the systems were considered equilibrated and suitable for statistical analysis. For the calculation of protein-lipid hydrogen bonds, a cutoff angle of 20° between the donor-hydrogen-acceptor atoms and a cutoff distance of 3.2 Å between the donor and acceptor atoms were applied. The snapshots of the different poses were created with Maestro's implementation of PyMol and Visual Molecular Dynamics (Schrödinger Release 2017-1: Maestro; Schrödinger) (Humphrey et al., 1996) and the UCSF Chimera package (Pettersen et al., 2004). MD simulations were run in workstations and an Advanced Research Information System supercomputer using the GPU implementation and parallel CPU algorithms of MD simulation codes as provided by Desmond [Schrödinger Release 2017-1: Desmond Molecular Dynamics System (D. E. Shaw Research) and Maestro-Desmond Interoperability Tools (Schrödinger)].

Computation of Relative Binding Free Energies by the MM-GBSA Continuum Solvation Approach. Relative binding free energies of aminoadamantane compounds were estimated by the 1-trajectory MM-GBSA approach (Homeyer and Gohlke, 2012) using the relevant module in Schrödinger Suite (Schrödinger Release 2017-1: Maestro; Schrödinger). Effective binding energies ($\Delta G_{effective}$) (Homeyer and Gohlke, 2012; Homeyer et al., 2016) were computed considering the gas phase energy and solvation free energy contributions to binding. $\Delta G_{effective}$ values were calculated by performing two independent MD simulations for each complex. For this, structural ensembles were extracted in intervals of 20 ps from the last 20 ns of the production simulations of the AM2-ligand complexes. Prior to the calculations, all water molecules, ions, and lipids were removed, and the structures were positioned such that the geometric center of AM2 was located at the coordinate origin. Molecular mechanics energies and the nonpolar contribution to the solvation free energy were calculated. The polar part of the solvation free energy was determined by generalized born calculations (Holst and Saied, 1993, 1995; Baker et al., 2001). In these calculations, a dielectric constant of $\varepsilon_{solute} = 1$ was assigned to AM2. Using an implicit solvent representation for the calculation of the effective binding energy is an approximation to reduce the computational costs of the calculations. Previous studies reported on differences in the number of direct interactions of the amino group of different aminoadamantane compounds with waters (Gkeka et al., 2013; Ioannidis et al., 2016). In the present work, it was valid to use this approximation because relative water accessibilities of the acceptor groups of the ligand with an orientation of the polar head toward the N end or the C end were similar. Entropy effects were ignored and assumed to be similar for the complexes of ligand **4** with the two proteins AM2 S31N and AM2 S31N/L46P and **1** with AM2 WT and AM2 L46P.

Results

Resistance Selection against the AM2 S31N Inhibitor 4. Hypothesis-driven optimization of the pharmacokinetic properties of isoxazole-conjugated AM2 S31N inhibitors led to the development of compound **4** (Wang et al., 2018). Electrophysiological assays showed that compound **4** blocked the AM2 S31N proton channel with a K_d of 4.5 ± 1.0 μM (Wang et al., 2018). In antiviral plaque assays, compound **4** inhibited multiple oseltamivir-sensitive and -resistant influenza A viruses with submicromolar EC_{50} values. Compound **4** was also well tolerated in MDCK cells having low cytotoxicity ($CC_{50} > 300$ μM) and had favorable in vitro pharmacokinetic properties, showing a half-life greater than 145 minutes in mouse microsomes and high membrane permeability in Caco-2 cells (Wang et al., 2018). Unlike previously designed AM2 S31N inhibitors, compound **4** was found to have slow K_{on} and K_{off} values in kinetic studies. To profile the drug-resistance mechanism of this newly developed inhibitor, the 2009 H1N1 pandemic virus A/California/07/2009 (H1N1) was passaged under increasing drug selection pressure of compound **4**. This virus is among the circulating influenza strains resistant to amantadine. In the passage experiment, the initial drug concentration was set as 1 × EC_{50} concentration as determined using plaque-reduction assays. For passage 0 virus (P0), no plaques were observed at 30 μM compound **4**. At passage 04 (P4), the drug selection pressure was set at 8 × EC_{50}. When compound **4** was tested against P4 viruses, several plaques were observed in the presence of 30 μM **4**, compared with no plaques for the P0, passage 02, or passage 03 viruses (Fig. 3; Table 1), indicating the emergence of resistance. Although resistant viruses appeared at P4, there was still a noticeable reduction in the overall number of plaques compared with the virus only. Therefore, the calculated EC_{50} remained unchanged (Fig. 3B; Table 1). At passage

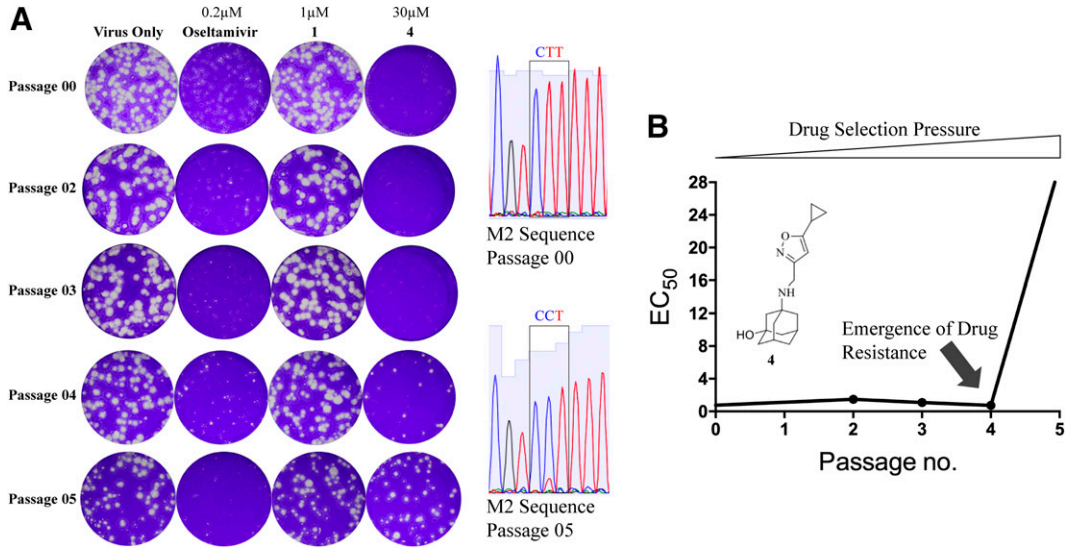

Fig. 3. Drug resistance for compound **4** selected in cell culture. (A) Viruses from each passage were tested against compound **4** at 30 μM using plaque-reduction assay to determine drug susceptibility. The M2 gene was sequenced from passage 00 (original virus stock) and passage 05 (virus that appears resistant to compound **4**) to map the mutations that give rise to resistance. CTT represents the nucleotide sequence for the lysine residue at position 46, and CCT represents the nucleotide sequence for the proline mutant identified in passage 05. (B) EC_{50} was determined for passages 02–05. At passage 05, the EC_{50} was observed to be >30 μM. All antiviral EC_{50} values are the mean ± S.D. of two independent experiments.

05 (P5), the drug selection pressure was increased to 16 × EC_{50}. The P5 virus showed drastic resistance, as a significant amount of plaques remained in the presence of 30 μM compound **4** (Fig. 3).

To determine the resistance mutation, the P5 viral gene segment that encodes for the AM2 channel was sequenced. Compared with the P0 virus which only had the S31N mutation, the P5 virus had an additional mutation, L46P, located at the end of the AM2 transmembrane helices. To rule out the possibility that other mutations existed in the viral genome that might influence drug sensitivity, whole-genome sequencing was performed for the P5 virus. Only the L46P mutation in the AM2 segment was found in P5 viruses when compared with the whole-genome sequence of the P0 viruses. AM2 S31N/L46P was found in less than 0.01% of clinically isolated human influenza A viruses in the Influenza Research Database (http://www.fludb.org) (data not shown), suggesting that L46P is a rare mutant among circulating viruses. Nevertheless, the presence of L46P in the database means that this mutant may exist naturally independent of drug selection pressure. Interestingly, the L46P mutation was no longer observed in the sequenced AM2 gene when the P5-resistant viruses underwent three additional passages in the absence of compound **4** (Table 1). Therefore, this mutation might not be favored in the absence of drug pressure.

Electrophysiological Assay Confirmed Drug Resistance of AM2 S31N/L46P against Compound 4. Electrophysiological TEVC measurements have been previously used as a reliable and robust tool to evaluate the function and inhibition of AM2 as well as the pharmacological properties of AM2 channel blockers. As expected, 100 μM amantadine (**1**) displayed marginal inhibition against the AM2 S31N (Wang et al., 2013a), whereas AM2 S31N inhibitors (compounds **2**–**6**) showed 47.9%–90.6% inhibition at the 2-minute time point after application (Li et al., 2017; Wang et al., 2018) (Fig. 4A, left column).

To investigate the AM2 S31N/L46P channel conductance and inhibition, the mutation was introduced in the pGEM3

TABLE 1
Drug-resistance selection

Passage Number[a]	Compound **4** Selection Pressure	EC_{50}[b]	Mutation[c]
	μM	μM	
0	N/A	0.8 ± 0.05	WT
1	0.75	N.D.	N.D.
2	1.5	1.5 ± 0.4	N.D.
3	3	1.1 ± 0.3	N.D.
4	6	0.7 ± 0.4	N.D.
5	12	>30 (resistant)	P46L
6	24	N.D.	P46L
7	0	N.D.	N.D.
8	0	N.D.	L46 + P46
9	0	N.D.	P46L

N/A, not applicable; N.D., not determined.
[a]Influenza Virus A/California/07/2009 (H1N1) was passaged at an MOI of 0.001 in MDCK cells.
[b]EC_{50} values were determined by plaque assay (mean ± S.D. of two independent experiments).
[c]The M segment encoding for the AM2 protein was sequenced.

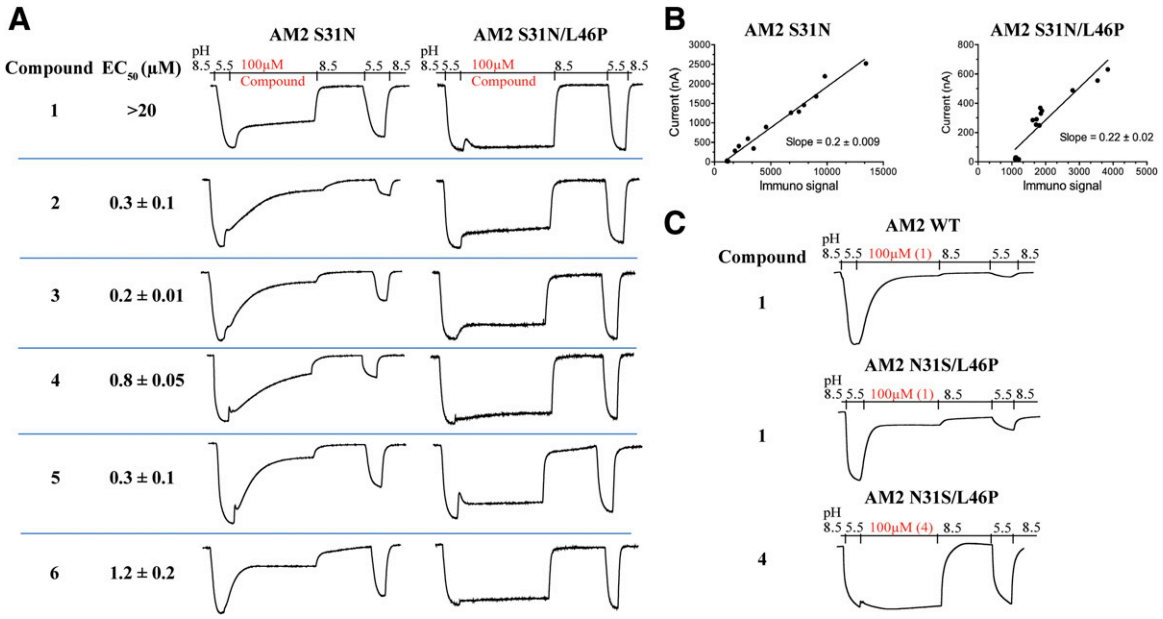

Fig. 4. TEVC recordings confirm the functional resistance of AM2 S31N/L46P toward S31N inhibitors. (A) Cell culture EC_{50} values against AM2 S31N–containing influenza viruses for compounds **1** (Wang et al., 2013a), **2**–**5** (Wang et al., 2018) and **6** (Li et al., 2017) are shown. Ion channel conductance of the AM2 S31N (left column traces) and AM2 S31N/L46P (right column traces) was measured in the presence of 100 μM for compounds **1**–**6**. (B) Specific activities were obtained by plotting the whole-cell current for single intact oocytes against the concentration of AM2 protein detected by immunofluorescence on the oocyte surface. (C) TEVC measurements for AM2 WT and AM2 L46P channels against compound **1** and AM2 L46P channel against compound **4**.

vector. In agreement with the drug-resistance selection, compounds **2–6** showed almost no inhibition on the proton conductance of AM2 S31N/L46P channels (Fig. 4A, right column). Specific conductance measurements were carried out to determine the effects on function due to the introduction of the L46P mutation. The current was plotted against the immunosignal to obtain a slope that correlates with the specific conductance. Overall, no significant change in proton conductance profile was observed between AM2 S31N channels and the mutated AM2 S31N/L46P (Fig. 4B), suggesting AM2 S31N/L46P remains a proton-selective channel.

To determine whether L46P affects the drug sensitivity of amantadine (**1**), the AM2 L46P mutant was constructed. As previously reported, amantadine (**1**) significantly inhibits WT channels, having 92.9% inhibition against 100 μM compound concentration at the 2-minute time point (Fig. 4C). Interestingly, it was found that the L46P in WT channels did not significantly change amantadine sensitivity with 91% inhibition. Compound **4** was unable to inhibit AM2 L46P channels, as shown in the comparison of conductance plots for **1** against AM2 WT and AM2 L46P and **4** against AM2 L46P (Fig. 4C). These results suggest that L46P disproportionally affects the drug sensitivity of AM2 S31N inhibitors **2–6** against the AM2 S31N channel but not the drug sensitivity of amantadine against AM2 WT.

MD Simulations of the Effect of L46P Mutant on Drug Binding. MD simulations were applied for the *apo* AM2 WT, AM2 S31N, and the corresponding mutated *apo* proteins AM2 L46P and AM2 S31N/L46P for 1 μs to investigate the conformational properties of these proteins. The MD simulations showed that the L46P induced a γ-turn in local structure. The peptide bond dihedral connecting R45 and L46 which was −172° in AM2 WT and AM2 S31N changed to +1.6° for AM2 L46P and AM2 S31N/L46P. Thus, the L46P mutation produced an important conformational change at the C end for each AM2 monomer. However, this change occurred simultaneously for all monomers, rendering the relative orientation between successive AM2 monomers the same as in the L46 case. The L46P mutation also affected more distant conformational changes in the AM2 TM part of the channel, with the most important for drug action being a broadening of the N terminus. This conformational change was observed after 350–400 ns in the 1-μs MD simulation of the *apo* protein AM2 S31N/L46P. The 1-μs equilibrated AM2 S31N and AM2 S31N/L46P proteins were then simulated for another 100 ns in complex with compound **4**. In both protein-drug complexes, the system reached equilibration after ~70 ns (Fig. 5).

In complexes of compound **4** with AM2 S31N or AM2 S31N/L46P proteins, the polar head of the ligand was oriented toward the N terminus according to experimental findings (Wang et al., 2013b; Wu et al., 2014; Hu et al., 2018). Ligand was stabilized with similar hydrophilic interactions in both complexes but different hydrophobic interactions. For the AM2 S31N–**4** complex, the adamantane ring fit close to Gly34, and the ligand formed hydrogen bond interactions between 1) its NH_2^+ group and isoxazole nitrogen and N31 amino side chains throughout the trajectory and 2) its hydroxyl group and, occasionally, the backbone Ala30 carbonyls (Fig. 5, A and B). The same hydrophilic interactions also stabilized compound **4** inside the AM2 S31N/L46P pore (Fig. 5C). However, there was a notable difference with regard to the hydrophobic interactions. In the AM2 S31N–**4** complex, the isoxazole-cyclopropyl fragment of compound **4** forms hydrophobic interactions with V27 side chain isopropyl groups. This hydrophobic interaction was lost in the AM2 S31N/L46P mutant due to the channel broadening at the N terminus between residues 22 and 31. Superposition between AM2 S31N and AM2 S31N/L46P complexes with compound

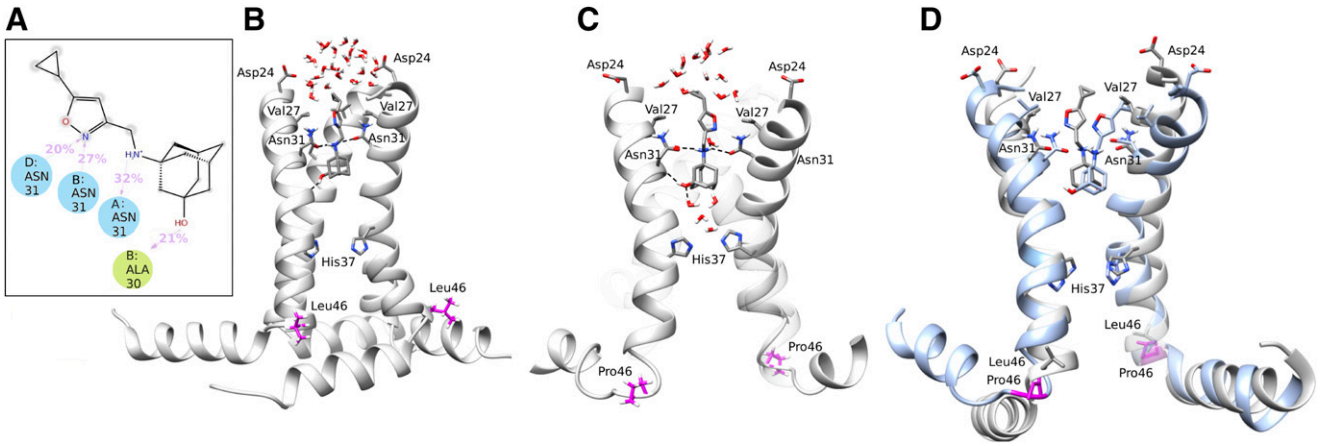

Fig. 5. MD simulation structures for compound **4** bound to AM2 S31N and AM2 S31N/L46P channels. (A) Two-dimensional diagram of the most important interactions between compound **4** and the AM2 S31N (22–62) from the 100-ns MD simulation trajectory. (B) In AM2 S31N (22–62) in complex with compound **4**, no water passage was observed between the ligand and N end, which is consistent with proton blockage. (C) AM2 S31N/L46P (22–62) in complex with compound **4**. The L46P mutation produced an N-end broadening that weakened key hydrophobic interactions between V27 residues and the isoxazole-cyclopropyl group of compound **4**. (D) Superposition of AM2 S31N (gray) and AM2 S31N/L46P (blue) structures with **4** bound.

4 clearly revealed this conformational change that the L46P mutation effected (Fig. 5D). The AM2 S31N/L46P mutant pore seems to broaden significantly between residues 22 and 31 compared with the AM2 S31N counterpart, making compound **4** unable to prevent the water molecules from entering the pore (Fig. 5C).

MM-GBSA binding free energy calculations from two independent MD simulations resulted in a more negative $\Delta G_{effective}$ for the AM2 S31N–**4** complex by more than 22.2 kcal mol^{-1} compared with the AM2 S31N/L46P–**4** complex (Table 2), suggesting a considerably more stable complex for **4** to AM2 S31N.

Next, MD simulations were applied for AM2 WT and AM2 L46P in complex with amantadine (Fig. 6). While AM2 S31N and AM2 S31N/L46P mutants showed differential drug sensitivity toward compound **4**, amantadine readily blocked both the AM2 WT and AM2 L46P mutants according to the MD simulations (Fig. 6, A and B). This observation was consistent with the electrophysiological results in which amantadine showed potent channel inhibition against AM2 WT and AM2 L46P (Fig. 4C). Interestingly, although L46P similarly broadened the channel pore at the N terminus in the AM2 L46P mutant, it only affected residues 22–31 and not residues 31–34, where amantadine binds. Indeed, in the MD simulations of AM2 L46P with amantadine, no water was observed to pass through the channel (Fig. 6B). Consequently, superposition between AM2 WT and AM2 L46P complexes showed similar interactions, stabilizing amantadine (Fig. 6C). MM-GBSA calculations from two independent MD simulations resulted in $\Delta G_{effective}$ values for **1** bound to AM2 WT and AM2 L46P that differed by less than 4 kcal mol^{-1}. This difference in binding energy value corresponds to the accuracy of the calculation method and suggests that the binding affinities are similar (Table 2).

Discussion

The conjugates of amantadine and polar head heterocycles represent useful leads for a new generation of anti-influenza A drugs. In this study, serial viral passaging experiments were performed to select escape variants that are resistant to one of our advanced lead compounds, **4**. Unlike previously identified drug-resistant AM2 mutants which had mutations along the N terminus of the channel between residues 26 and 34, a novel drug-resistant mutation was identified, L46P, which is located at the C end of the AM2 transmembrane helices and is distal from the drug-binding site of the N terminus of the channel pore. Drug resistance of the AM2 S31N/L46P mutant against compound **4** was confirmed in both the electrophysiological assay and the antiviral plaque assay. Interestingly, AM2 L46P remained sensitive to amantadine. To elucidate the differential effect of L46P on the drug sensitivity of AM2 S31N inhibitor **4** and AM2 WT inhibitor amantadine, MD simulations and MM-GBSA calculations were performed on these protein ligand complexes. The mutation found at L46P broadened the drug-binding site at the N terminus of the channel, specifically between residues 22 and 31, in both the AM2 L46P and AM2 S31N/L46P mutants. However, this only affects the binding of AM2 S31N inhibitors such as compound **4**, as it abolished the critical hydrophobic interaction between the lipophilic heterocyclic part of the drug and V27 side chains. In contrast, the L46P mutation had minimal effect on amantadine binding, as this compound binds between residues 31 and 34, which was not altered in pore diameter due to

TABLE 2
MM-GBSA–calculated free energy of binding

AM2 Channel[a]	$\Delta G_{effective}$[b]
	kcal·mol^{-1}
Compound **1**	
WT	−36.3 ± 2.5
L46P	−40.2 ± 2.5
Compound **4**	
S31N	−64.1 ± 2.5
S31N/L46P	−41.9 ± 2.1

[a]AM2: ligand structures were simulated as described in the main text.
[b]Binding free energies ± S.D. from two independent MD simulations for each complex.

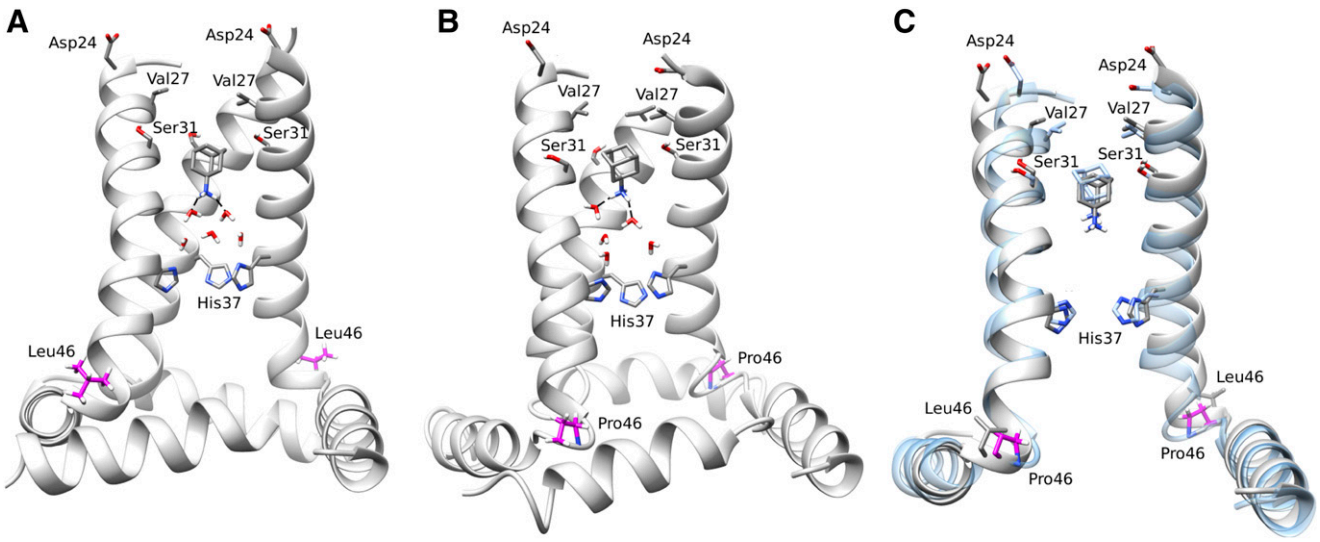

Fig. 6. MD simulation structures for amantadine (**1**) bound to AM2 WT and AM2 L46P channels. AM2 WT (A) and AM2 L46P (B) in complex with amantadine (**1**) located near residues 31–34 within the pore. Amantadine prevented the entrance of waters from the N end of AM2 L46P. (C) Superposition of AM2 WT (gray) and AM2 L46P (blue) with amantadine (**1**) bound. AM2 L46P is wider than AM2 WT in the N end, but they are equally as wide in the C end, enabling amantadine to block protons passage.

the L46P mutation. In other words, L46P affected the region beyond the amantadine-binding site. Overall, MD simulations and MM-GBSA calculations provided an explanation for this allosteric resistance mechanism. To our knowledge, L46P is the first drug-resistant AM2 mutant located below H37 that was experimentally confirmed.

It should be noted that Santer et al. (2018a,b) recently reported only marginal inhibition of AM2 L46P by amantadine in a proton flux (pHlux) assay in AM2-expressing *Escherichia coli*. In their study, AM2 with random mutations was expressed in *E. coli*, and the proton flux and drug sensitivity were quantified using the pH-sensitive green fluorescent protein, pHluorin. In their results, it was shown that a single L46P mutant was resistant to amantadine and a few other analogs. Intriguingly, the M2 variant M_060, which contained two extra V7L/G16C mutants in the N terminus other than L46P, displayed amantadine sensitivity similar to what we observed in our L46P alone using an A/California/07/09 background. It appears that amantadine showed sequence-dependent drug sensitivities for N31S/L46P variants in their bacteria flux assay. It was also noted that two potent AM2 V27A channel blockers developed by us, spiro[5.5]undecan-3-ylmethanamine and spiro[5.5]undecan-3-amine (Balannik et al., 2009), had minimal channel inhibition when tested in their bacteria flux assay against the AM2 V27A single mutant. Taken together, the bacteria flux assay results appear to be not consistent with the TEVC and antiviral assay results, which raises a concern of whether the bacteria flux assay can be applied to accurately characterize channel blockage and predict the antiviral efficacy of M2 channel blockers. We cannot provide an accurate explanation for this discrepancy since we do not know the exact experimental details of the bacteria flux assay. One reason might be that the differences in the lipid composition between *E. coli* and *Xenopus* oocyte membranes contribute to the method-specific variations in the activity and inhibition profiles (Zhou and Cross, 2013). Moreover, the transporters and channels expressed in *E. coli* might compromise the assay results. Nevertheless, our electrophysiological assay results showed that AM2 L46P mutant remained sensitive to amantadine, and this result was also supported by the MD simulation and MM-GBSA calculations.

The design of successful antiviral therapeutics requires consideration and evaluation for the likelihood of resistance, since a substandard barrier to resistance can derail the development of an otherwise efficacious drug candidate. The drivers of drug resistance depend on the inhibitor as well as the protein target. For AM2, the allowed amino acid changes that still preserve the functionality of the protein necessary for viral replication appear to be limited, as studied by Balannik et al. (2010). It likely correlates that drug resistance for new AM2 inhibitors are limited to a subset of mutant variants. Up until now, drug-resistance selection in viral passage experiments has identified amino acid changes at or near the drug-binding site. The newly identified L46P AM2 in replicating viruses represents a new resistance strategy that influenza can adopt when under drug selection pressure. In regard to AM2 antiviral development, the next generation of AM2 S31N inhibitor might need to focus on the region between S31 and H37 to avoid the allosteric effect of the L46P mutant. Moreover, the disappearance of the L46P mutation after drug withdrawal as well as its low abundance in circulating strain populations suggest that strains containing this AM2 variant may have limited persistence. The reason for this remains unclear, as we did not observe any changes in the proton conductance activity of L46P AM2 channels. Moreover, additional research is needed to evaluate whether compensatory mutations can arise that may increase persistence. An important point to be considered in future drug-discovery campaigns is how subtle changes in the overall structure of AM2 can have dramatic effects on the efficacy of developing drugs. Because the lipid composition can influence membrane protein structure, the advent of improved structural biology techniques that can resolve native-like conformations will greatly aid in the design of future channel blockers.

Acknowledgments

This work was supported by computational time granted from the Greek Research and Technology Network in the National High Performance Computing facility—Advanced Research Information System—under project ID pr005010.

Authorship Contributions

Participated in research design: Musharrafieh, Ma, Kolocouris, Wang.

Conducted experiments: Musharrafieh, Lagarias, Ma, Tan.

Contributed new reagents or analytic tools: Musharrafieh, Lagarias, Ma, Tan, Kolocouris, Wang.

Performed data analysis: Musharrafieh, Lagarias, Ma, Tan, Kolocouris, Wang.

Wrote or contributed to the writing of the manuscript: Musharrafieh, Kolocouris, Wang.

References

Acharya R, Carnevale V, Fiorin G, Levine BG, Polishchuk AL, Balannik V, Samish I, Lamb RA, Pinto LH, DeGrado WF, et al. (2010) Structure and mechanism of proton transport through the transmembrane tetrameric M2 protein bundle of the influenza A virus. *Proc Natl Acad Sci USA* **107**:15075–15080.

Baker NA, Sept D, Joseph S, Holst MJ, and McCammon JA (2001) Electrostatics of nanosystems: application to microtubules and the ribosome. *Proc Natl Acad Sci USA* **98**:10037–10041.

Balannik V, Carnevale V, Fiorin G, Levine BG, Lamb RA, Klein ML, Degrado WF, and Pinto LH (2010) Functional studies and modeling of pore-lining residue mutants of the influenza a virus M2 ion channel. *Biochemistry* **49**:696–708.

Balannik V, Wang J, Ohigashi Y, Jing X, Magavern E, Lamb RA, Degrado WF, and Pinto LH (2009) Design and pharmacological characterization of inhibitors of amantadine-resistant mutants of the M2 ion channel of influenza A virus. *Biochemistry* **48**:11872–11882.

Best RB, Zhu X, Shim J, Lopes PEM, Mittal J, Feig M, and Mackerell AD Jr (2012) Optimization of the additive CHARMM all-atom protein force field targeting improved sampling of the backbone ϕ, ψ and side-chain $\chi(1)$ and $\chi(2)$ dihedral angles. *J Chem Theory Comput* **8**:3257–3273.

Bowers KJS, Chow E, Xu H, Dror RO, Eastwood MP, Gregersen BA, Klepesis JL, Kolossvary I, Moraes MA, Sacerdoti FD, et al. (2006) Molecular dynamics—scalable algorithms for molecular dynamics simulations on commodity clusters, in *Proceedings of the 2006 ACM/IEEE conference on Supercomputing*; 2006 Nov 11–17; Tampa, FL, pp 84, ACM Press, New York.

Cady SD and Hong M (2008) Amantadine-induced conformational and dynamical changes of the influenza M2 transmembrane proton channel. *Proc Natl Acad Sci USA* **105**:1483–1488.

Cady SD, Schmidt-Rohr K, Wang J, Soto CS, Degrado WF, and Hong M (2010) Structure of the amantadine binding site of influenza M2 proton channels in lipid bilayers. *Nature* **463**:689–692.

Chen BJ, Leser GP, Jackson D, and Lamb RA (2008) The influenza virus M2 protein cytoplasmic tail interacts with the M1 protein and influences virus assembly at the site of virus budding. *J Virol* **82**:10059–10070.

Darden T, York D, and Pedersen L (1993) Particle mesh Ewald: an Nlog(N) method for Ewald sums in large systems. *J Chem Phys* **98**:10089–10092.

Essmann U, Perera L, Berkowitz ML, Darden T, Lee H, and Pedersen LG (1995) A smooth particle mesh Ewald method. *J Chem Phys* **103**:8577–8593.

Gkeka P, Eleftheratos S, Kolocouris A, and Cournia Z (2013) Free energy calculations reveal the origin of binding preference for aminoadamantane blockers of influenza A/M2TM pore. *J Chem Theory Comput* **9**:1272–1281.

Halgren TA (1996) Merck molecular force field. 1. Basis, form, scope, parameterization, and performance of MMFF94. *J Comput Chem* **17**:490–519.

Holst M and Saied F (1993) Multigrid solution of the Poisson - Boltzmann equation. *J Comput Chem* **14**:105–113.

Holst MJ and Saied F (1995) Numerical solution of the nonlinear Poisson–Boltzmann equation: developing more robust and efficient methods. *J Comput Chem* **16**: 337–364.

Homeyer N and Gohlke H (2012) Free energy calculations by the molecular mechanics Poisson-Boltzmann surface area method. *Mol Inform* **31**:114–122.

Homeyer N, Ioannidis H, Kolarov F, Gauglitz G, Zikos C, Kolocouris A, and Gohlke H (2016) Interpreting thermodynamic profiles of aminoadamantane compounds inhibiting the M2 proton channel of influenza A by free energy calculations. *J Chem Inf Model* **56**:110–126.

Hu F, Luo W, and Hong M (2010) Mechanisms of proton conduction and gating in influenza M2 proton channels from solid-state NMR. *Science* **330**:505–508.

Hu Y, Hau RK, Wang Y, Tuohy P, Zhang Y, Xu S, Ma C, and Wang J (2018) Structure-property relationship studies of influenza A virus AM2-S31N proton channel blockers. *ACS Med Chem Lett* **9**:1111–1116.

Humphrey W, Dalke A, and Schulten K (1996) VMD: visual molecular dynamics. *J Mol Graph* **14**:33–38, 27–28.

Humphreys DD, Friesner RA, and Berne BJ (1994) A multiple-time-step molecular dynamics algorithm for macromolecules. *J Phys Chem* **98**:6885–6892.

Ioannidis H, Drakopoulos A, Tzitzoglaki C, Homeyer N, Kolarov F, Gkeka P, Freudenberger K, Liolios C, Gauglitz G, Cournia Z, et al. (2016) Alchemical free energy calculations and isothermal titration calorimetry measurements of aminoadamantanes bound to the closed state of influenza A/M2TM. *J Chem Inf Model* **56**: 862–876.

Jing X, Ma C, Ohigashi Y, Oliveira FA, Jardetzky TS, Pinto LH, and Lamb RA (2008) Functional studies indicate amantadine binds to the pore of the influenza A virus M2 proton-selective ion channel. *Proc Natl Acad Sci USA* **105**:10967–10972.

Jones G, Willett P, Glen RC, Leach AR, and Taylor R (1997) Development and validation of a genetic algorithm for flexible docking. *J Mol Biol* **267**:727–748.

Jorgensen WL, Chandrasekhar J, Madura JD, Impey RW, and Klein ML (1983) Comparison of simple potential functions for simulating liquid water. *J Chem Phys* **79**:926–935.

Koynova R and Caffrey M (1998) Phases and phase transitions of the phosphatidylcholines. [published correction appears in *Biochim Biophys Acta* (2001) 1513: 82]. *Biochim Biophys Acta* **1376**:91–145.

Kwon B and Hong M (2016) The influenza M2 ectodomain regulates the conformational equilibria of the transmembrane proton channel: insights from solid-state nuclear magnetic resonance. *Biochemistry* **55**:5387–5397.

Li F, Hu Y, Wang Y, Ma C, and Wang J (2017) Expeditious lead optimization of isoxazole-containing influenza A virus M2-S31N inhibitors using the Suzuki-Miyaura cross-coupling reaction. *J Med Chem* **60**:1580–1590.

Lyman E and Zuckerman DM (2006) Ensemble-based convergence analysis of biomolecular trajectories. *Biophys J* **91**:164–172.

Ma C, Fiorin G, Carnevale V, Wang J, Lamb RA, Klein ML, Wu Y, Pinto LH, and DeGrado WF (2013) Asp44 stabilizes the Trp41 gate of the M2 proton channel of influenza A virus. *Structure* **21**:2033–2041.

Ma C, Polishchuk AL, Ohigashi Y, Stouffer AL, Schön A, Magavern E, Jing X, Lear JD, Freire E, Lamb RA, et al. (2009) Identification of the functional core of the influenza A virus A/M2 proton-selective ion channel. *Proc Natl Acad Sci USA* **106**: 12283–12288.

Ma C and Wang J (2018) Functional studies reveal the similarities and differences between AM2 and BM2 proton channels from influenza viruses. *Biochim Biophys Acta Biomembr* **1860**:272–280.

Ma C, Zhang J, and Wang J (2016) Pharmacological characterization of the spectrum of antiviral activity and genetic barrier to drug resistance of M2-S31N channel blockers. *Mol Pharmacol* **90**:188–198.

Martyna GJ, Tobias DJ, and Klein ML (1994) Constant pressure molecular dynamics algorithms. *J Chem Phys* **101**:4177–4189.

McCown MF and Pekosz A (2006) Distinct domains of the influenza a virus M2 protein cytoplasmic tail mediate binding to the M1 protein and facilitate infectious virus production. *J Virol* **80**:8178–8189.

Musharrafieh R, Ma C, and Wang J (2018) Profiling the in vitro drug-resistance mechanism of influenza A viruses towards the AM2-S31N proton channel blockers. *Antiviral Res* **153**:10–22.

Park EK, Castrucci MR, Portner A, and Kawaoka Y (1998) The M2 ectodomain is important for its incorporation into influenza A virions. *J Virol* **72**:2449–2455.

Pettersen EF, Goddard TD, Huang CC, Couch GS, Greenblatt DM, Meng EC, and Ferrin TE (2004) UCSF Chimera--a visualization system for exploratory research and analysis. *J Comput Chem* **25**:1605–1612.

Pinto LH, Holsinger LJ, and Lamb RA (1992) Influenza virus M2 protein has ion channel activity. *Cell* **69**:517–528.

Rossman JS, Jing X, Leser GP, and Lamb RA (2010) Influenza virus M2 protein mediates ESCRT-independent membrane scission. *Cell* **142**:902–913.

Ryckaert JP, Ciccotti G, and Berendsen HJC (1977) Numerical integration of the cartesian equations of motion of a system with constraints: molecular dynamics of N-alkanes. *J Comput Phys* **23**:327–341.

Santner P, Martins JMDS, Kampmeyer C, Hartmann-Petersen R, Laursen JS, Stein A, Olsen CA, Arkin IT, Winther JR, Willemoës M, et al. (2018a) Random mutagenesis analysis of the influenza A M2 proton channel reveals novel resistance mutants. *Biochemistry* **57**:5957–5968.

Santner P, Martins JMDS, Laursen JS, Behrendt L, Riber L, Olsen CA, Arkin IT, Winther JR, Willemoës M, and Lindorff-Larsen K (2018b) A robust proton flux (pHlux) assay for studying the function and inhibition of the influenza a M2 proton channel. *Biochemistry* **57**:5949–5956.

Schmidt NW, Mishra A, Wang J, DeGrado WF, and Wong GCL (2013) Influenza virus A M2 protein generates negative Gaussian membrane curvature necessary for budding and scission. *J Am Chem Soc* **135**:13710–13719.

Sharma M, Yi M, Dong H, Qin H, Peterson E, Busath DD, Zhou HX, and Cross TA (2010) Insight into the mechanism of the influenza A proton channel from a structure in a lipid bilayer. *Science* **330**:509–512.

Stouffer AL, Acharya R, Salom D, Levine AS, Di Costanzo L, Soto CS, Tereshko V, Nanda V, Stayrook S, and DeGrado WF (2008) Structural basis for the function and inhibition of an influenza virus proton channel. [published correction appears in *Nature* (2008) 452:380]. *Nature* **451**:596–599.

Takeda M, Pekosz A, Shuck K, Pinto LH, and Lamb RA (2002) Influenza a virus M2 ion channel activity is essential for efficient replication in tissue culture. *J Virol* **76**: 1391–1399.

Tang Y, Zaitseva F, Lamb RA, and Pinto LH (2002) The gate of the influenza virus M2 proton channel is formed by a single tryptophan residue. *J Biol Chem* **277**: 39880–39886.

Thomaston JL, Polizzi NF, Konstantinidi A, Wang J, Kolocouris A, and DeGrado WF (2018) Inhibitors of the M2 proton channel engage and disrupt transmembrane networks of hydrogen-bonded waters. *J Am Chem Soc* **140**:15219–15226.

Verdonk ML, Chessari G, Cole JC, Hartshorn MJ, Murray CW, Nissink JWM, Taylor RD, and Taylor R (2005) Modeling water molecules in protein-ligand docking using GOLD. *J Med Chem* **48**:6504–6515.

Wang J (2016) M2 as a target to combat influenza drug resistance: what does the evidence say?. *Future Virol* **11**:1–4.

Wang J, Li F, and Ma C (2015) Recent progress in designing inhibitors that target the drug-resistant M2 proton channels from the influenza A viruses. *Biopolymers* **104**: 291–309.

Wang J, Ma C, Wang J, Jo H, Canturk B, Fiorin G, Pinto LH, Lamb RA, Klein ML, and DeGrado WF (2013a) Discovery of novel dual inhibitors of the wild-type and the most prevalent drug-resistant mutant, S31N, of the M2 proton channel from influenza A virus. *J Med Chem* **56**:2804–2812.

Wang J, Wu Y, Ma C, Fiorin G, Wang J, Pinto LH, Lamb RA, Klein ML, and Degrado WF (2013b) Structure and inhibition of the drug-resistant S31N mutant of the M2 ion channel of influenza A virus. *Proc Natl Acad Sci USA* **110**:1315–1320.

Wang Y, Hu Y, Xu S, Zhang Y, Musharrafieh R, Hau RK, Ma C, and Wang J (2018) In vitro pharmacokinetic optimizations of AM2-S31N channel blockers led to the discovery of slow-binding inhibitors with potent antiviral activity against drug-resistant influenza A viruses. *J Med Chem* **61**:1074–1085.

Wu Y, Canturk B, Jo H, Ma C, Gianti E, Klein ML, Pinto LH, Lamb RA, Fiorin G, Wang J, et al. (2014) Flipping in the pore: discovery of dual inhibitors that bind in different orientations to the wild-type versus the amantadine-resistant S31N mutant of the influenza A virus M2 proton channel. *J Am Chem Soc* **136**:17987–17995.

Zhou HX and Cross TA (2013) Modeling the membrane environment has implications for membrane protein structure and function: influenza A M2 protein. *Protein Sci* **22**:381–394.

Address correspondence to: Dr. Antonios Kolocouris, National and Kapodistrian University of Athens, Panepistimiopolis-Zografou 15771, Greece. E-mail: ankol@pharm.uoa.gr; or Dr. Jun Wang, University of Arizona, 1657 E. Helen St, BIO5 Institute Room 303, Tucson, AZ 85721. E-mail: junwang@pharmacy.arizona.edu